ARA Journal, Vol. 2000-2002, No. 25-27

State-of-the-Art Aircraft Icing and Anti-Icing Simulation

Farooq Saeed
Research Associate, J.-A. Bombardier Aeronautical Chair
École Polytechnique de Montréal, Département de Génie Mécanique
C. P. 6079, Succ. Centre-Ville, Montréal, Québec, H3C 3A7, Canada
farooq.saeed@polymtl.ca

Abstract: The paper gives a brief description of the various state-of-the-art mathematical models used to simulate ice accretion and anti-icing simulation on an aircraft wing section. These models are implemented in the CANICE code. CANICE results from a typical icing and anti-icing simulation are presented in comparison with available experimental data and another icing code, LEWICE. The paper also discusses the usefulness of CANICE in reliably predicting ice accretion and in assessing anti-icing heat requirements for given flight and atmospheric conditions. The anti-icing system is modeled after a hot-air jet impinging on a flat plate from which the internal heat transfer coefficients are obtained. The optimum hot-air mass flux needed to avoid icing can be obtained by coupling the CANICE code with an optimization code.
Keywords: Aircraft icing, anti-icing, droplet trajectories, panel method, optimization.

Nomenclature

A_T, B_T, C_T = coefficients of a second order polynomial
A_c = cross-section area of metal skin, m^2
c = airfoil chord, m
d = droplet diameter, m
F = shear force, N/m^2
h_{anti} = heat transfer coefficient between the anti-icing hot air and the metal skin, $W/(m^2K)$
$\overline{h}_{anti}$ = average heat transfer coefficient between the anti-icing hot air and the metal skin, $W/(m^2K)$
H = jet nozzle-to-surface spacing, m
k = thermal conductivity, W/(mK)
$\dot{m}$ = mass flow rate, kg/s
$\dot{m}''_{imp}$ = mass flow rate per unit area of water caught, $kg/(m^2s)$
$\overline{Nu}$ = $\overline{h}_{anti}\,2W/k$, average Nusselt number
Nu_x = $h_{anti}\,2W/k$, local Nusselt number
P = pressure, N/m^2
Pr = Prandtl number
Q_{anti} = heat flux provided by the anti-icing device to the metal skin, W/m^2
Q_{wall} = heat flux lost by the metal skin to the external flow, W/m^2
Re_{jet} = $V_{jet}\,2W/\nu$, jet Reynolds number
R_V = $V_\infty\,d/\nu$, free-stream droplet Reynolds number
s = curvilinear distance from stagnation point, m
s_{in} = curvilinear distance from jet impinging point, m
T = temperature, K
T_{jet} = average temperature of jet at nozzle exit, K
T_w = temperature in the water film, K
T_{wall} = surface temperature on the inner side of the metal skin, K
u_w = water film velocity, m/s
u_{imp} = droplet velocity at impact, m/s
V_{jet} = average velocity of jet at nozzle exit, m/s
V_∞ = free-stream velocity, m/s
W = jet nozzle slot width, m
x, y = spatial coordinates, m
δ = water film thickness, m
μ_w = dynamic viscosity of water, $N.s/m^2$
τ_w = shear stress at the wall, N/m^2

1. Introduction

Atmospheric icing presents a major hazard to aircraft operating under natural icing conditions and is a cause of major concerns for the certification authorities as well as the aircraft manufacturers. The steady rise in the global aviation traffic means an increased likelihood of encountering natural icing conditions. This suggest an increased frequency of icing related accidents unless a considerable amount of effort is focused on the various safety issues concerning in-flight aircraft icing, such as efficient design of ice protection related systems. In-flight icing usually occurs during the take-off or landing phase of a flight, when the aircraft have to fly through clouds and the temperatures are at or below freezing point. During these phases, the high-lift devices, such as slats or flaps, are deployed in an almost fully extended configuration. It, therefore, becomes essential for the aircraft manufacturers to have the necessary tools to simulate ice accretion and determine the anti-icing requirements for these phases of flight to meet any eventuality and, thus, to certify aircrafts for flight under icing conditions.

To enhance flight safety under natural icing conditions, FAA has recently initiated a multi-year icing plan [1, 2] to address the various issues related to in-flight aircraft icing. One of the several key tasks outlined in the plan is the continued development of icing simulation methods to ensure their validity and reliability. In an effort to support the objectives of the FAA Icing Plan, and facilitate *Bombardier Aerospace* in the certification process, the main focus of research under the *J.-A.*

Bombardier Aeronautical Chair at École Polytechnique, Montréal, has been the development of a reliable ice accretion and anti-icing simulation code CANICE [3-13] for single/multi-element airfoils and complete wing configurations. In this paper, the overall computational procedure used in CANICE is presented next with the aid of an ice accretion and anti-icing simulation example. Afterwards, a procedure for the optimization of anti-icing heat requirements is also discussed. Finally, the paper ends with some brief conclusions.

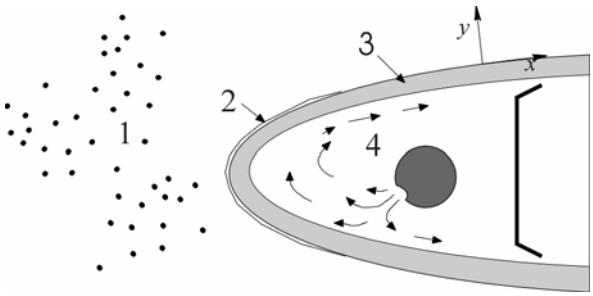

Fig. 1. Various modules used in the mathematical formulation of an ice accretion simulation code: (1) External flowfield, (2) Surface thermodynamics, (3) Conduction through metal skin, and (4) Anti-icing hot-air jet region.

2. Computational Procedure

This section presents the overall mathematical model used to simulate the physical process of ice accretion as implemented in the CANICE code. The mathematical model is divided into various modules that are briefly described below (see Fig. 1).

2.1 Inviscid external flow field

The external flow field module includes computation of the external airflow around the airfoil. First, a potential solution (inviscid) for the flow around the single/multi-element airfoil is determined using the method of Hess and Smith [14]. The solution is based on the Laplace equation:

$$\nabla^2 \phi = 0 \qquad (1)$$

with $V = V_\infty$ as the far field boundary condition, a solid wall boundary condition along the airfoil surface and the Kutta condition at the trailing edge of the airfoil. The airfoil surface is represented by several straight line segments called panels on which a distribution of sources, sinks, and/or vorticity is imposed, the solution of which yields the velocity field $V = \nabla \phi(x, y)$. The Karman-Tsien compressibility correction is applied to the flow field. The flow solution is reliable for low Mach number (M < 0.5) and small angles of attack (α < 10 deg.).

2.2 Viscous boundary-layer analysis

The skin-friction and heat transfer coefficients along the airfoil surface are found with the help of an integral boundary-layer method that accounts for roughness effects due to presence of ice. The solution is based on the method of Pohlhausen [15]. The equations used to solve the boundary layer by the integral method have been presented in previous papers [4, 9]. The presence of ice on the airfoil leading edge causes transition from laminar to turbulent flow as in the case of a rough surface [16] and is assumed to occur when $Re_k \geq 600$ where $Re_k = V_k k_s/\nu$, V_k = velocity at roughness height and k_s = the equivalent sand-grain roughness height. Several methods [17-25] have been proposed to determine the equivalent sand-grain roughness height k_s for iced surfaces. Once k_s is known, the turbulent skin-friction and heat-transfer coefficients for rough surfaces can be obtained by empirical relations proposed by Dipprey and Sabersky [26] and others [27, 28]. For laminar heat-transfer coefficient, the relation proposed by Smith and Spalding [29] is generally used.

2.3 Water-droplet trajectories

The water droplet trajectories, starting in the unperturbed region of the flow, are then found, based on the drag force exerted by the potential flow velocity field, the droplet inertia and the gravity force [30-33]. In non-dimensional form, assuming that the effect of gravity is negligible, the basic trajectory equation is:

$$\left(\frac{K}{C_D R/24} \right) \ddot{\mathrm{x}} = V - \dot{\mathrm{x}} \qquad (2)$$

where **x** represents the dimensionless droplet position and the dot represents the derivative with respect to dimensionless time. Thus the trajectory depends upon the inertia parameter K, the droplet drag C_D and droplet Reynolds number R. Bragg [33] has shown that the term in parenthesis can be approximated by a single parameter, the modified inertia parameter K_O:

$$K_O = 18\,K\left[R_V^{-2/3} - \left(\frac{\sqrt{6}}{R_V} \right) \mathrm{Arctan}\left(\frac{R_V^{1/3}}{\sqrt{6}} \right) \right] \qquad (3)$$

where R_V is the free-stream droplet Reynolds number. For a given droplet diameter d in terms of the median volumetric diameter (MVD), Eq. (2) is solved with the help of a forth-order Runge-Kutta scheme [recipies] to obtain droplet trajectories that impinge on the airfoil surface. From the droplet impingement distribution, the local impingement/catch efficiencies β (= dy/ds) are calculated as shown in Fig. 2. Then the mass rate of water caught on each airfoil panel is

$$\dot{m}_{imp} = \beta V_\infty \mathrm{LWC}\, ds \qquad (4)$$

where LWC is the liquid water content in the air. The complete procedure is described in detail in Ref. [8].

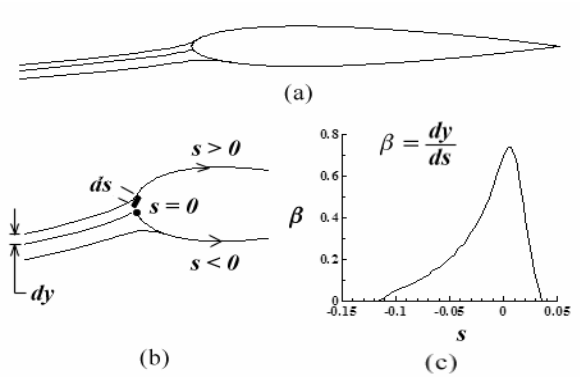

Fig. 2. (a) Water-droplet trajectories, (b) Close-up view and nomenclature, and (c) A typical local impingement efficiency β curve.

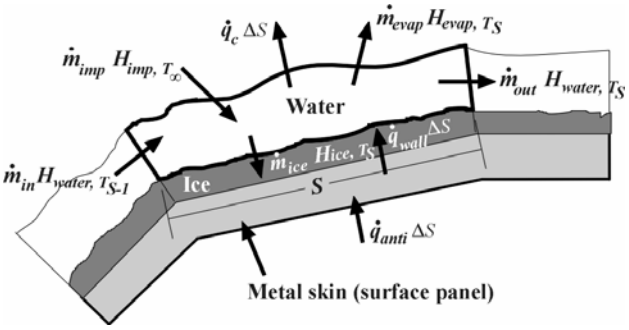

Fig. 3. The control volume for mass and energy conservation.

2.4 Thermodynamic analysis

The impinging super-cooled droplets, depending upon surface temperature, may either coalesce into larger surface drops under the influence of surface tension and flow along the surface under the influence of aerodynamic shear forces due to the airflow or freeze on the surface or shed off the surface. The ice layer formed by the initial freezing forms a rough surface that enhances the convective heat transfer and local impingement efficiency of the surface and further aids in the ice accretion process. The freezing process due to the impact of super-cooled droplets on a surface, in icing conditions, was first studied by Messinger [34]. He introduced the concept of freezing fraction *f* by a thermodynamic analysis of the temperature of an unheated surface in icing conditions.

The thermodynamic analysis is based on the first law of thermodynamics that states that the mass and energy flux must be balanced in a control volume (*cv*) on the surface. Thus, a single or several control volumes are placed over a single surface panel that extends from the airfoil surface to the outside of the boundary layer (Fig. 3). The conservation of mass requires that the mass flux entering the control volume must equal the mass flux leaving the control volume, that is

$$\dot{m}_{imp} + \dot{m}_{in} = \dot{m}_{ice} + \dot{m}_{evap} + \dot{m}_{out} \tag{5}$$

where $\dot{m}_{imp}$ is the mass flux of the impinging water entering the control volume, $\dot{m}_{in}$ is mass flux of water flowing into the control volume from the downstream control volume (*s*-1), $\dot{m}_{ice}$ is the mass rate of ice being accumulated, $\dot{m}_{evap}$ is the mass flux of water loss through evaporation and $\dot{m}_{out}$ is mass flux of water leaving the control volume in upstream direction. The freezing fraction is defined as the fraction of the total mass flux entering the control volume that freezes, that is

$$f = \dot{m}_{ice} / (\dot{m}_{imp} + \dot{m}_{in}) \tag{6}$$

Similarly the conservation of energy flux through the same control volume can be expressed in terms of total enthalpy *H* and heat source $\dot{q}$ as:

$$\begin{aligned} &\dot{m}_{imp} H_{water,T_\infty} + \dot{m}_{in} H_{water,T_{s-1}} + \dot{q}_{wall}\Delta s = \\ &\dot{m}_{ice} H_{ice,T_s} + \dot{m}_{evap} H_{vapor,T_s} + \dot{m}_{out} H_{water,T_s} + \dot{q}_c \Delta s \end{aligned} \tag{7}$$

where

$$\begin{aligned} H_{water,T_\infty} &= C_{p,water}(T_\infty - 273.15) + V_\infty^2/2 \\ H_{water,T_{s-1}} &= C_{p,water}(T_{s-1} - 273.15) \\ H_{ice,T_s} &= C_{p,ice}(T_s - 273.15) - L_f \\ H_{vapor,T_s} &= C_{p,water}(T_s - 273.15) - L_v \end{aligned} \tag{8}$$

L_f is the latent heat of fusion, L_v is the latent heat of evaporation, $\dot{q}_{wall}$ is the heat flux through the airfoil surface and $\dot{q}_c$ is the convective heat flux due to the airflow and the kinetic heating of the surface through friction, that is

$$\dot{q}_c = h_c\left(T_s - T_e - V_e^2/2C_{p,air}\right) \tag{9}$$

where h_c is the local heat-transfer coefficient for a rough surface.

The modified model and improved computational procedure for the thermodynamic analysis is dealt in detail in Refs. [4, 6, 17-21, 35]. A brief description of the procedure is outlined here. First, Eqs. (5) and (6) are substituted in Eq. (7). The two unknowns in the resulting equation are the surface temperature T_s and the freezing fraction *f*. The procedure is then to set T_s = 273.15 K and evaluate *f*. If $f < 0$, it implies that the surface temperature is greater than 273.15 K so then set $f = 0$ and re-calculate T_s. If $0 \le f \le 1$, it implies that the initial assumption was correct and if $f > 1$, it implies that the surface temperature is less than 273.15 K, so then set $f = 1$ and re-calculate T_s. The calculation of T_s requires an iterative process that is continued until two successive values of T_s are very close

to each other. Once T_s and f are known, then $\dot{m}_{ice}$, $\dot{m}_{evap}$, and $\dot{m}_{out}$ are found for each control volume from Eq. (6).

2.5 Geometry update

The height of ice growth $\Delta y_{ice,s}$ on each surface panel during a given time interval Δt is determined from

$$\Delta y_{ice,s} = \dot{m}_{ice} \Delta t \Delta s / \rho_{ice} \tag{10}$$

where ρ_{ice} is the density of ice. These $\Delta y_{ice,s}$ increments are then added normal to the surface panels to produce a new surface profile. It should be pointed out that since the surface panels are at an angle to each other, addition of large amounts of ice normal to panels leads to unrealistic ice shapes. In order to overcome this fact, different ice growth strategies [21, 24, 36, 37], such as re-paneling of surface geometry by restricting panel size, angle and density, and number of control volumes per surface panel based on surface curvature and application of an ice mass conservation scheme to distribute a fraction of total ice mass on a panel in the empty regions in between the panels, must be employed to ensure smooth ice growth.

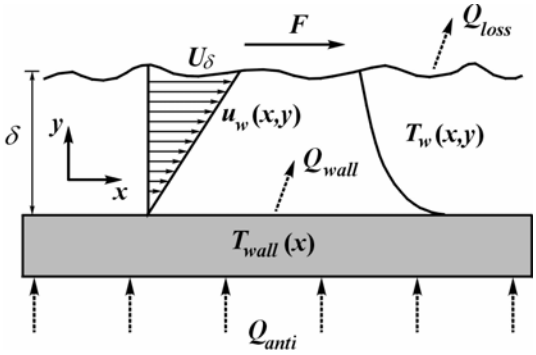

Fig. 4. Water-runback model [9].

2.6 Water runback

The mass flux of water leaving the control volume in upstream direction, $\dot{m}_{out}$, is treated as runback. The runback water is modeled as a continuous film flow [9-12] with no waves on the airfoil surface (Fig. 4). The equation used to model the velocity distribution in the water film is:

$$u_w(x,y) = \frac{1}{2\mu_w}\frac{dP}{dx}y^2 + \frac{1}{\mu_w}\left(F - \delta(x)\frac{dP}{dx}\right)y \tag{11}$$

The potential flow solution of the external air region gives the value for the pressure gradient. The shear force F, applied by the external flow region, drives the film flow. The shear force F is the sum of the wall friction, τ_{air}, exerted by the boundary layer and of the momentum per unit area from incoming water droplets:

$$F = \tau_{air} + \dot{m}''_{imp} u_{imp} \tag{12}$$

Because the water velocity at air-liquid interface is much lower than the air velocity at the edge of the boundary layer, the shear force at the interface is found by solving the equations for a boundary layer over a fixed wall. The temperature distribution in the water film is approximated by a second order polynomial:

$$T_w(x,y) = A_T(x)\,y^2 + B_T(x)\,y + C_T(x) \tag{13}$$

The heat flux coming from the wall, Q_{wall}, and the heat flux lost to the external airflow, Q_{loss},, respectively give the temperature slope at the wall and at the air-water interface. With the help of these quantities, values for the polynomial coefficients A_T and B_T are found. The heat flux lost to the airflow includes convection, evaporation and the energy losses to warm the impinging droplets. For a water mass flow rate $\dot{m}$, the bulk temperature, T_b, inside the water film sets the $C_T(x)$ value.

Comparisons with numerical results of Al-Khalil [38] have shown the validity of the model for a very thin film flow.

2.7 Solid wall

For a thin plate made of a material with uniform conductivity k and cross surface area A_c, the temperature variation across the thickness can be neglected. Thus, only conduction along the airfoil surface is considered for the airfoil wall. The airfoil wall essentially redistributes the heat coming from the anti-icing system Q_{anti}:

$$Q_{wall} = Q_{anti} + kA_c \frac{dT_{wall}}{dx^2} \tag{14}$$

2.8 Anti-icing simulation

Several kinds of in-flight ice protection systems can be used to prevent ice accretion on airfoil critical surfaces [39]. Here, an anti-icing system based on a hot-air jet similar to the one being used on Bombardier aircraft is presented. Hot air circulation inside the leading edge region of the wing provides the necessary heat to avoid ice accretion. The amount of heat is sufficient enough to evaporate most of the water in the leading edge region. The liquid water is treated as runback that freezes to form ice at some downstream location. In the case of a multi-element airfoil, the anti-icing hot air is used to remove ice from the first element (slat) only.

The anti-icing hot air region is modeled with a local internal heat transfer coefficient h_{anti}. The local heat transfer coefficient is calculated from empirical relation [40] for the average Nusselt number $\overline{Nu}$ for a jet impinging on a flat plate, that is:

$$\frac{\overline{Nu}}{\mathrm{Pr}^{0.42}} = \frac{3.06}{x/W + H/W + 2.78}\mathrm{Re}^m \tag{15}$$

$$m = 0.695 - \left(\frac{x}{2W} + \left(\frac{H}{2W} \right)^{1.33} + 3.06 \right)^{-1} \qquad (16)$$

where x is the distance from the jet impingement point on the flat plate, H is the distance between the jet nozzle-to-surface (flat plate) spacing, W is the jet nozzle slot width and, $Re = V_{jet}\ 2W/\nu$ is the jet Reynolds number, $\overline{Nu} = \overline{h}_{anti}\ 2W/k$ is the average Nusselt number, $\overline{h}_{anti}$ the average heat transfer coefficient, V_{jet} the average jet velocity at nozzle exit. The relation (15) is valid for

$$\begin{aligned} 3000 &\le Re_{jet} \le 90000 \\ 2 &\le H/W \le 10 \\ 4 &\le x/W \le 20 \end{aligned} \qquad (17)$$

and yields a bell-shaped curve for which Nu_x monotonously decays from a maximum value at the stagnation point of the jet. It is then used to determine the local heat transfer coefficients inside the airfoil. For a given hot-air mass flow rate, the jet Reynolds number is fixed and thus the average Nusselt number is known. The Nu_x distribution for a jet Reynolds number of 89,300 and H/W = 8 is shown in Fig. 5

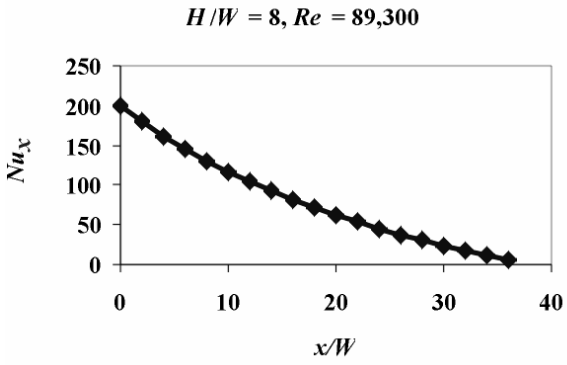

Fig. 5. The Nu_x distribution for a jet Reynolds number of 89,300 and H/W = 8.

Once the heat transfer coefficient h_{anti} is known from Nu_x distribution, heat flux coming from the anti-icing system is evaluated with the help of the exit temperature of the jet, T_{jet}, and the local airfoil skin temperature, T_{wall}:

$$Q_{anti} = h_{anti}(T_{jet} - T_{wall}) \qquad (18)$$

The internal heat transfer coefficients are found with the curvilinear distance, S_{in} , from the jet impinging point to the center of each panel. For each panel, the corresponding heat transfer coefficient at the same distance on a flat plate is used. The airfoil wall is divided into control volumes of panel length and of thickness of the airfoil skin to solve Eq. (14). The surface temperature and the amount of water that evaporates for a given internal heat transfer coefficient distribution are found by an iterative procedure.

An initial surface temperature distribution is first used to obtain the heat flux Q_{anti} from the anti-icing device. Then, the heat flux coming out from the airfoil wall, Q_{wall}, is calculated with the help of the assumed wall temperature distribution. This heat flux is used to find the new surface temperatures, T_{wall}. The heat flux Q_{anti}, from the anti-icing hot air region corresponding to this surface temperature distribution is then evaluated again and used to calculate the new surface temperatures. The iterative process stops when energy entering the airfoil wall equals energy leaving the airfoil metal skin. Relaxation is needed for convergence of this iterative procedure.

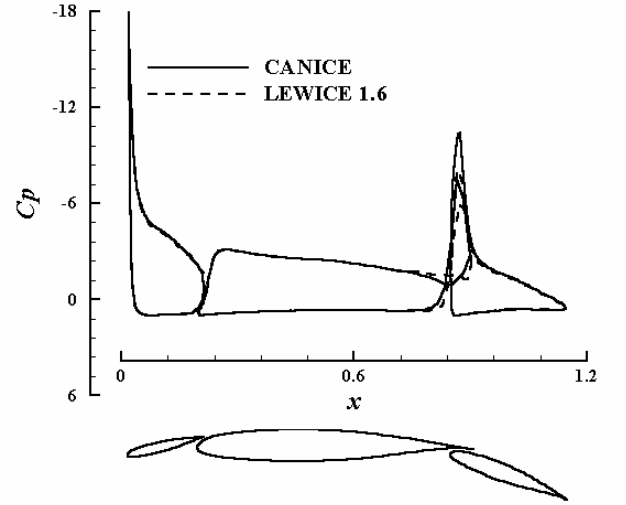

Fig. 6. A three-element airfoil chosen for the study and the comparison of pressure coefficient C_p distribution at α = 6 deg.

3. Results

A three-element (slat, main and flap) airfoil shown in Fig. 6 was used for icing and anti-icing simulation. Ice accretion results obtained with CANICE are first compared with available numerical results from LEWICE [21]. Then, an anti-icing device is simulated in the slat and the effect of mass flow rate on ice accretion rate is determined.

Figure 6 also shows a comparison of pressure coefficient distribution *Cp* obtained from the solution of the potential flow about the three-element airfoil at an angle of attack α = 6 deg. The *Cp* distributions are similar except between the main element and the flap. These differences between *Cp* values indicate that the flow fields predicted in those regions are different.

3.1 Ice accretion simulation

For the icing and anti-icing cases considered here, the same atmospheric conditions are used. The airfoil is flying at an altitude of 580.6 m, with an angle of attack α = 6 deg, a velocity of 90 m/s, an ambient temperature of -10°C and a Reynolds number, based on chord length, of 6.52 million. The liquid water content (*LWC*) in the cloud is 0.54 g/m^3

and the mean volumetric diameter (*MVD*) is 20μm. An icing duration of 6 minutes is considered.

Fig. 7. Water-droplet trajectories impinging on the three-element airfoil.

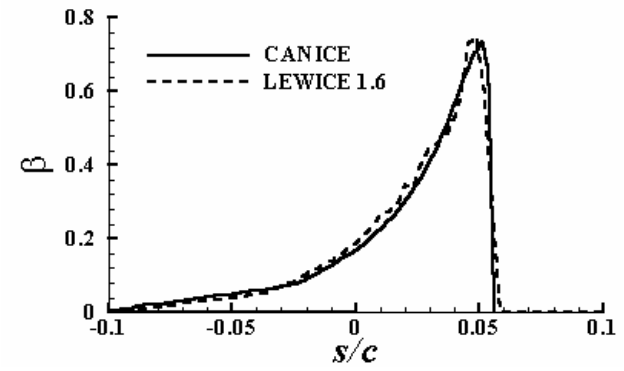

Fig. 8. Comparison of impingement efficiencies for the slat (leading element).

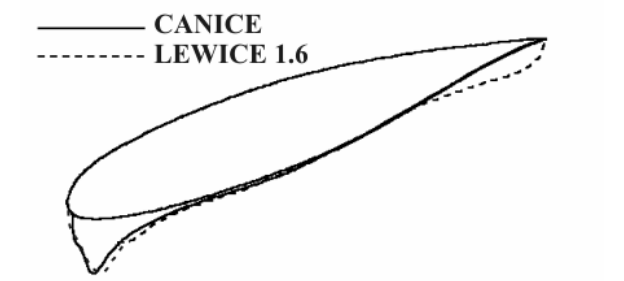

Fig. 9. Comparison of ice shapes on slat (leading element).

Figure 7 shows the water-droplet trajectories that impact the airfoil surface computed by CANICE. Impingement efficiencies predicted by CANICE and LEWICE for the slat (leading element) are plotted as a function of curvilinear abscissa *s/c* in Fig. 8. The ice shapes comparison is shown in Fig. 9. Ice shapes on the first element are not similar in CANICE and LEWICE calculations because of the differences in the impingement efficiencies. Fig. 10 shows another case of ice accretion simulation in comparison with experiment and several state-of-the-art icing codes from a NATO exercise [37].

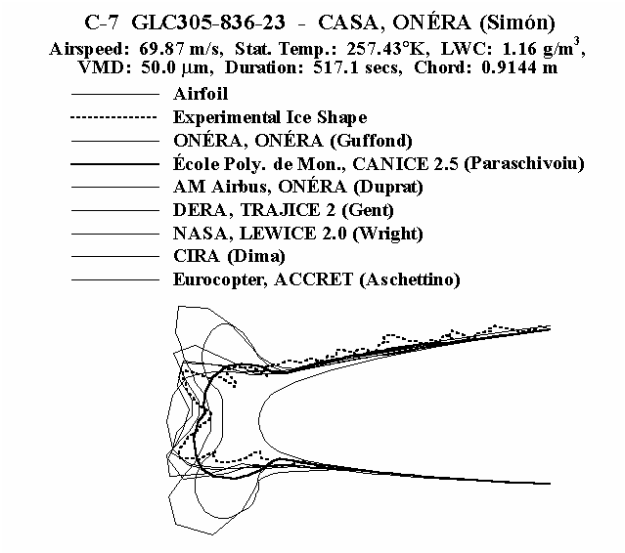

Fig. 10. Comparison of ice shapes prediction by several state-of-the-art icing codes [37].

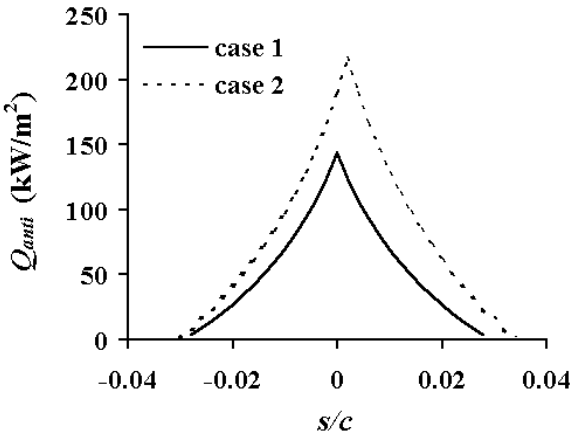

Fig. 11. The anti-icing heat flux provided to the metal skin.

3.2 Anti-icing simulation

An anti-icing device is simulated in the slat of the three-element airfoil with the same atmospheric conditions as in the ice accretion case. The metal skin is assumed to be of 2 mm thick aluminum with a thermal conductivity of 100W/(mK). Hot air is injected through a 1mm slot at a temperature of 170°C. Two anti-icing simulation cases are performed, with two different hot-air mass flow rates and two different jet-impingement points on the inner surface of the slat. In the first case, a mass flow rate of 0.0003 kg/s/m span is used while for the second case, a mass flow rate of 0.0012 kg/s/m span is used. Figure 11 shows the heat flux provided to the metal skin by the hot-air jet. The higher the mass flow rate, the higher is the heat flux. In the second case, the impinging point is moved towards the upper part of the airfoil. A total power of 7782W is

delivered by the anti-icing device in the first case compared to 14182W in the second case.

In the two cases, the water is not entirely evaporated on the first element. In the first case 45% of the water is evaporated and, in the second case, 65% of the water is evaporated. Some water runbacks and freezes downstream of the impingement limits. Figure 12 shows the resulting ice shapes after application of the anti-icing hot air for one minute of ice accretion.

The external heat transfer coefficients calculated by the integral boundary layer method reach a maximum near the leading edge of the airfoil. The maximum is so high, around 4000 W/(mK), that it is almost impossible to avoid ice accretion there. The water freezes almost instantaneously there. This is why the ice shapes obtained are a little strange. The external heat transfer coefficients calculated are doubtful because separation should probably occur near the leading edge.

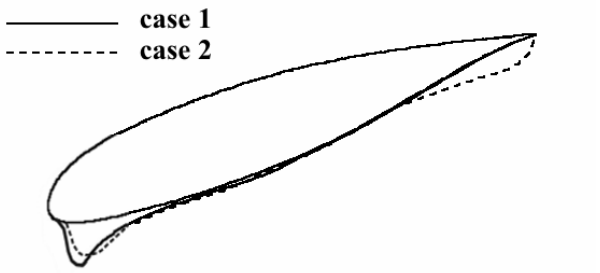

Fig. 11. The resulting ice shape after applying the anti-icing heat flux.

4. Conclusion

The paper gives a brief description of the various state-of-the-art mathematical models used to simulate ice accretion and anti-icing simulation on an aircraft wing section. These models are implemented in the CANICE code. CANICE results from a typical icing and anti-icing simulation are presented in comparison with available experimental data and another icing code, LEWICE. The results indicate the usefulness of CANICE in reliably predicting ice accretion and in assessing anti-icing heat requirements for given flight and atmospheric conditions. The optimum hot-air mass flux needed to avoid icing can be obtained by coupling the CANICE code with an optimization code. This study is currently underway at École Polytechnique.

Acknowledgments

The authors would like to acknowledge the support of NSERC through a cooperative Research and Development Grant with Bombardier Aerospace and the help of F. Tezok. The first author would also like to thank the FCAR for his financial support.

References

[1] Federal Aviation Administration, *Proceedings of the FAA International Conference on Aircraft In-Flight Icing*, Vol. I and II, Springfield, Virginia, USA, May 6—8, 1996. Final Report.

[2] United States Department of Transportation, Federal Aviation Administration. *FAA In-Flight Icing Plan*, Springfield, Virginia, USA, April 1997.

[3] Brahimi, M. T., Tran, P., and Paraschivoiu, I., *Numerical Simulation and Thermodynamic Analysis of Ice Accretion on Aircraft Wings*, Technical Report C. D. T. C159, École Polytechnique de Montréal, Montréal, Canada, May 1994.

[4] Paraschivoiu, I., Tran, P. and Brahimi, M. T., "Prediction of the Ice Accretion with Viscous Effects on Aircraft Wings," *AIAA Journal of Aircraft*, 31(4), 855, 1994.

[5] Tran, P., Brahimi, M. T. and Paraschivoiu, I., "Ice Accretion on Aircraft Wings," *Canadian Aeronautics and Space Journal*, 40(3), 185, 1994.

[6] Tran, P., Brahimi, M. T., Paraschivoiu, I., Pueyo, A., and Tezok, F., "Ice Accretion on Aircraft Wings with Thermodynamic Effects," *AIAA Journal of Aircraft*, 32(2), 444, 1995.

[7] Tran, P., Brahimi, M. T., Tezok, F, and Paraschivoiu, I., "On the Modelling of Ice Accretion on Single and Multi-Element Airfoils," *Intl. Icing Symposium '95*, École Polytechnique de Montréal, pp. 367-378, 1995.

[8] Brahimi, M. T., Tran, P., Chocron, D., Tezok, F., and Paraschivoiu, I., "Effect of Supercooled Large Droplets on Ice Accretion Characteristics," AIAA Paper 97-0306, 1997.

[9] Morency, F., Brahimi, M. T., Tezok, F., and Paraschivoiu, I., "Hot Air Anti-Icing System Modelization in the Ice Prediction Code CANICE," AIAA Paper 98-0192, 1998.

[10] Morency, F., Tezok, F., and Paraschivoiu, I., "Heat and Mass Transfer in the Case of an Anti-icing System Modelisation," AIAA Paper 99-0623, 1999.

[11] Morency, F., Tessier, P., Saeed, F., and Paraschivoiu, I., "Anti-Icing System Simulation on Multi-Element Airfoil," 46th Annual Conference of Canadian Aeronautics and Space Institute (CASI), Montréal, Canada, pp. 463—470, May 1999.

[12] Morency, F., Tezok, F. and Paraschivoiu, I., "Anti-Icing System Simulation Using CANICE," *AIAA Journal of Aircraft*, 36(6), 999, 1999.

[13] Saeed, F., Morency, F. and Paraschivoiu, I., "Numerical Simulation of a Hot-Air Anti-Icing System," AIAA Paper 2000-0630, 2000.

[14] Hess, J. L., and Smith, A. M. O., "Calculation of Potential Flow about Arbitrary Bodies," *Progress in Aeronautical Sciences*, 8:1-138, D. Kuchemann (editor), Elmsford, New York, Pergmon Press, 1967.

[15] Schlichting, H., Boundary Layer Theory, F. J. Cerra (editor), Mc-Graw Hill, New York, 1979.

[16] Von Doenhoff, A. E., and Horton, E. A., "Low Speed Experimental Investigation of the Effect of Sandpaper Type Roughness on Boundary-Layer Transition," NACA TN 3858, 1956.

[17] Ruff, G. A. and Berkowitz, B. M., *Users Manual for the NASA Lewis Ice Accretion Prediction Code (LEWICE)*, NASA CR-185129, May 1990.

[18] Shin, J., Berkowitz, B. M., Chen, H., and Cebeci, T., "Prediction of Ice Shapes and Their Effect on Airfoil Performance," AIAA Paper 91-0264, 1991.

[19] Cebeci, T., Chen, H. H., and Alemdaroglu, N., ``Fortified LEWICE with Viscous Effects," *Journal of Aircraft*, 28(9), Sept. 1991.

[20] Wright, W. B., *Update to the NASA Lewis Ice Accretion Code LEWICE*, NASA CR-195387, Oct. 1994.

[21] Wright, W. B., *Users Manual for the Improved NASA Lewis Ice Accretion Code LEWICE 1.6*, NASA CR-198355, June 1995.

[22] Shin, J., Wilcox, P., Chin, V., and Sheldon, D., "Icing Test Results on an Advanced Two-Dimensional High-Lift Multi-Element Airfoil," AIAA Paper 94-1869, 1994.

[23] Shin, J., "Characteristics of Surface Roughness Associated with Leading Edge Ice Accretion," NASA TM-106459, AIAA Paper 94-0799, 1994.

[24] Saeed, F., Gouttebroze, S., and Paraschivoiu, I., "Modified CANICE for Improved Prediction of Airfoil Ice Accretion," 8th Aerodynamic Symposium of 48th CASI Conference, Toronto, Canada, Apr. 29-- May 2, 2001.

[25] Havugimana, P.-C., Lutz, C., Saeed, F., Paraschivoiu, I., Kerevanian, G.-K., Sidorenko, A., Bernard, E., Cooper, R. K., and Raghunathan, R. S., "A Comparison of Skin Friction and Heat Transfer Prediction by Various Roughness Models," AIAA Paper 2002-3052, 2002.

[26] Dipprey, D. F., and Sabersky, R. H., "Heat and Momentum Transfer in Smooth and Rough Tubes at Various Prandtl Number," *International Journal of Heat and Mass Transfer*, 6, 1963.

[27] Kays, W. M., and Crawford, M. E., *Convective Heat and Mass Transfer*, 2nd edition, Mc-Graw-Hill, New York, 1980.

[28] Owen, P. R., and Thomson, W. R., "Heat Transfer Across Rough Wall Surfaces," *Journal of Fluid Mechanics*, 15, 1963.7

[29] Smith, A. G., and Spalding, D. B., "Heat Transfer in a Laminar Boundary Layer with Constant Fluid Properties and Constant Wall Temperature," *Journal of Royal Aeronautical Society*, 62, 60, 1958.

[30] Glauert, M., "A Method of Constructing the Paths of Raindrops of Different Diameters Moving in the Neighbourhood of (1) a Circular Cylinder, (2) an Aerofoil Placed in a Uniform Stream of Air; and Determination of the Rate of Deposit of the Drops on the Surface and the Percentage of Drops Caught," Aeronautical Research Council, UK, R & M 2025, Nov. 1940.

[31] Langmuir, I., and Blodgett, K. B., "A Mathematical Investigation of Water Droplet Trajectories," US Army Air Forces TR 5418, Feb. 1946 (Contract No. W-33-038-ac-9151 with General Electric Co.). Also US Department of Commerce Publication Board (PB) No. 27565.

[32] Bergrun, Norman R., "A Method for Numerically Calculating the Area and Distribution of Water Impingement on the Leading edge of an Airfoil in a Cloud," NACA TN 1397, Aug. 1947.

[33] Bragg, M. B., "A Similarity Analysis of the Droplet Trajectory Equation," *AIAA Journal*, 20(12), 1681, Dec. 1982.

[34] Messinger, B. L., "Equilibrium Temperature of an Unheated Icing Surface as a Function of Airspeed," *Journal of Aeronautical Sciences*, 20(1), 29, Jan. 1953.

[35] Macklin, W. C., and Payne, G. S., "A Theoretical Study of the Ice Accretion Process," *Quarterly Journal of the Royal Meteorological Society*, 93, 195, 1967.

[36] Pueyo, A., Chocron, D., and Kafyeke, F., "Improvements to the Ice Accretion Code CANICE," 8th Aerodynamic Symposium of 48th CASI Conference, Toronto, Canada, Apr. 29-- May 2, 2001.

[37] Gouttebroze, S., Saeed, F., and Paraschivoiu, I., "CANICE—Capabilities and Current Status," NATO/RTO Workshop, *Assessment of Icing Code Prediction Capabilities*, at CIRA, Capua, Italy, Dec. 6—7, 2000.

[38] Al-Khalil , K. M., *Numerical Simulation of an Aircraft Anti-Icing System Incorporating a Rivulet Model for the Runback Water*, Ph. D. thesis, University of Toledo, Toledo, Ohio, USA, June 1991.

[39] Thomas, S. K., Cassoni , R. P., and MacArthur, C. D., "Aircraft Anti-Icing and Deicing Techniques and Modeling," AIAA *Journal of Aircraft*, 33, 841, Sept.-Oct. 1996.

[40] Martin, H., "Heat and Mass Transfer Between Impinging Gas Jets and Solid Surface," *Advances in Heat Transfer*, 13, 1977.